On the approximation of the von Neumann equation in the semi-classical limit. Part I : numerical algorithm

Francis Filbet, François Golse

ON THE APPROXIMATION OF THE VON-NEUMANN EQUATION IN THE SEMI-CLASSICAL LIMIT. PART I : NUMERICAL ALGORITHM

FRANCIS FILBET AND FRANÇOIS GOLSE

Abstract. We propose a new approach to discretize the von Neumann equation, which is efficient in the semi-classical limit. This method is first based on the so called Weyl's variables to address the stiffness associated with the equation. Then, by applying a truncated Hermite expansion of the density operator, we successfully handle this stiffness. Additionally, we develop a finite volume approximation for practical implementation and conduct numerical simulations to illustrate the efficiency of our approach. This asymptotic preserving numerical approximation, combined with the use of Hermite polynomials, provides an efficient tool for solving the von Neumann equation in all regimes, near classical or not.

Keywords: Quantum mechanics, von Neumann equation, Hermite polynomial expansion.

Contents

1. Introduction 1
1.1. Quantum dynamics in Weyl's variables 3
1.2. Semi-classical limit 4
2. Hermite spectral method 6
2.1. Hermite approximation of the von Neumann equation 7
2.2. Review of error estimates 8
3. Finite volume in x and time discretization 9
3.1. Finite volume method 9
3.2. Approximation of the non-local term when $\hbar \ll 1$ 10
4. Numerical simulations 11
4.1. Harmonic potential 11
4.2. Quantum revivals 12
4.3. Quantum tunneling 15
4.4. The Morse potential 18
5. Conclusion 19
References 19

1. Introduction

We consider an operator $\hat{\rho}$, called the density-matrix operator, satisfying the Liouville-von Neumann or simply von Neumann equation in the operator formulation

$$\begin{cases} i\,\hbar\,\partial_t\hat{\rho} \,=\, [H,\hat{\rho}], \\ \hat{\rho}(0) \,=\, \hat{\rho}^{in}\,, \end{cases}$$

Date: May 21, 2024.
2020 *Mathematics Subject Classification.* Primary 35Q40, Secondary 65N08, 65N35 .

where $\hbar$ is the reduced Planck constant, H is the quantum mechanical Hamiltonian, for instance,

$$H = -\frac{\hbar^2}{2m}\Delta + V(X),$$

where V is a multiplication operator, *i.e.* $V\phi(X) = V(X)\phi(X)$ with V a real-valued function, and where $[H, \hat{\rho}] = H\,\hat{\rho} - \hat{\rho}\,H$ is the commutator. Here, we suppose that $\hat{\rho}(t)$ is a density operator on $L^2(\mathbb{R}^d)$, such that

$$\hat{\rho}(t)^* \,=\, \hat{\rho}(t) \,\geq\, 0\,, \quad \mathrm{Tr}(\hat{\rho}(t)) \,=\, 1, \quad t \geq 0.$$

In particular, $\hat{\rho}(t)$ is trace-class, and therefore Hilbert-Schmidt, hence by [9, Theorem 6.12], there exists a unique $\rho(t|\,X, Y) \in L^2_{X,Y}$, such that for any $\phi \in L^2(\mathbb{R}^d)$, we define $\hat{\rho}(t)\phi$ as the function

$$X \,\mapsto\, \hat{\rho}(t)\,\phi(X) \,=\, \int_{\mathbb{R}^d} \rho(t|\,X, Y)\,\phi(Y)\,\mathrm{d}Y\,.$$

Thus, the von Neumann equation can be written as follows for the function $(X, Y) \mapsto \rho(t|\,X, Y)$,

$$\left\{ \begin{array}{l} i\,\hbar\,\partial_t \rho(t|\,X, Y) \,=\, -\dfrac{\hbar^2}{2m}\,(\Delta_X \,-\, \Delta_Y)\,\rho(t|\,X, Y) \,+\, (V(X) \,-\, V(Y))\,\rho(t|\,X, Y)\,, \\ \\ \rho(0) \,=\, \rho^{in}\,. \end{array} \right. \tag{1.1}$$

The statement worth noting is that for $\hbar \ll 1$, the dynamics described by the von Neumann equation becomes stiff, leading to a multiscale problem. Thus a major challenge in quantum dynamics is to develop efficient numerical techniques capable of handling a large variety of wavelengths. For instance, numerical schemes used to solve the Schrödinger equation typically demand that both the time step Δt and mesh size, in the semiclassical regime when $\hbar \ll 1$, are of order $O(\hbar)$, or may even be smaller than $\hbar$ [22]. Actually, time splitting methods have the advantage of using large time steps when only the physical observables are concerned [2]. We also refer to [26, 27, 16, 25] and the references therein for the numerical approximation of the Schrödinger equation in the semiclassical limit. A fundamental concept to understand these mesh strategies is the Wigner transform, which serves as a useful tool for investigating the semiclassical limit of the Schrödinger equation. Additionally for the von Neumann equation, the density operator, which is Hermitian, positive semi-definite, and has trace equal to one by definition, should ideally maintain these properties at the discrete level in order to ensure realistic outcomes.

In this context, a first approach has been proposed in [14] and consists of successive application of short time propagators which are evaluated by using fast Fourier transforms. This method demonstrates high efficiency for short time when the density matrix is spatially localized but, unfortunately, it requires a small time step of order $\hbar$. Later in [3], the authors proposed a numerical scheme for a related model, again based on the Fourier pseudo-spectral method. It allows a description both in configuration as well as in momentum space. More recently, various structure preserving schemes have been studied to guarantee trace conservation and positivity of the discrete density matrix, allowing numerical simulations over large time intervals.

Actually, as we shall see more clearly later, the von Neumann equation is strongly related to the Wigner equation, which shares the same kind of numerical difficulties arising from the nonlocal and highly-oscillating pseudo-differential operator. It has been shown that the Wigner function can be discretized in a robust way using adaptive pseudo-spectral methods [31, 33]. In these methods, the carefully crafted spectral decomposition of the Wigner function enables the oscillatory components introduced by the Wigner kernel to be solved exactly. Finally, the oscillatory quantum effects can also be mitigated by decomposing the potential in a classical and quantum part [29, 30] or by reformulating the Wigner equation using spectral components of the force field [32].

Our aim is to design numerical schemes for the von Neumann equation (1.1) allowing an evaluation of the main observables (mass, momentum, and energy densities...) without having to use

time steps or space discretization in $O(\hbar)$. We already know that it is possible to choose time steps much larger than $\hbar$ and get error estimates uniform in $\hbar$ [2, 13] by applying time splitting schemes. But the discussion in [2, 13] leaves aside the space discretization issue, which is the core problem addressed here.

Our first move is to write the von Neumann equation in terms of Weyl's variables (see (1.2)). This removes all stiffness as $\hbar \ll 1$, and the new equation so obtained is well adapted to the semi-classical limit as $\hbar$ tends to zero. Then, in Section 2, we expand the density operator using Hermite polynomials leading to a spectrally accurate approximation. We shall briefly review error estimates, proven in our forthcoming work [10], which are uniform in the parameter $\hbar$. Next, in Section 3 we propose a finite volume scheme for the space discretization coupled with a Crank-Nicolson time discretization. Furthermore, in order to reduce the computational effort when $\hbar \ll 1$, we present an approximation of the non-local operator obtained after our change of variables. Finally, we perform extensive numerical simulations with various potentials in order to illustrate the efficiency of our numerical scheme (see Section 4).

1.1. **Quantum dynamics in Weyl's variables.** To remove the stiffness due to the parameter $\hbar$ in the von Neumann equation, the key idea consists in rewriting (1.1) in the new variables defined below, called "Weyl's variables":

$$\left\{ \begin{array}{l} x \,:=\, \dfrac{X \,+\, Y}{2}\,, \\ \\ y \,:=\, \dfrac{X \,-\, Y}{\hbar}\,, \end{array} \right. \tag{1.2}$$

which can be explicitly inverted as

$$X \,=\, x \,+\, \frac{\hbar}{2}\, y\,, \qquad Y \,=\, x \,-\, \frac{\hbar}{2}\, y\,.$$

Although this terminology is not common, it is obviously suggested by Weyl's quantization (see formula (1.1.9) of [18]). Hence, we set

$$R(t|\, x, y) \,:=\, \rho\,(t|\, X, Y)\;;$$

and find that ρ is solution to (1.1) if and only if R satisfies

$$\left\{ \begin{array}{l} i\,\hbar\,\partial_t R(t|\, x, y) \,=\, -\hbar \displaystyle\sum_{j=1}^{d} \partial_{x_j}\partial_{y_j} R(t|\, x, y) \,+\, \left(V\left(x + \frac{\hbar}{2}\, y\right) \,-\, V\left(x - \frac{\hbar}{2}\, y\right)\right) R(t|\, x, y)\,, \\ \\ R(0) \,=\, R^{in}_{\hbar}\,, \end{array} \right.$$

or equivalently

$$\left\{ \begin{array}{l} \partial_t R(t|\, x, y) \,=\, i \displaystyle\sum_{j=1}^{d} \partial_{x_j}\partial_{y_j} R(t|\, x, y) \,-\, i\frac{V\left(x + \frac{\hbar}{2}\, y\right) \,-\, V\left(x - \frac{\hbar}{2}\, y\right)}{\hbar}\, R(t|\, x, y)\,, \\ \\ R(0) \,=\, R^{in}_{\hbar}\,. \end{array} \right. \tag{1.3}$$

Let us first review some elementary properties on the operator $\hat{\rho}$ and their interpretation in terms of the function R. We first recall that $\hat{\rho}$ is a density operator on $L^2(\mathbb{R}^{2d})$, that is $\hat{\rho}(t)^* \,=\, \hat{\rho}(t)$, which means that R satisfies

$$R(t|\, x, -y) \,=\, \overline{R(t|\, x, y)}\,,$$

whereas the trace property becomes

$$\mathrm{Tr}\,(\hat{\rho}(t)) \,=\, \int_{\mathbb{R}^d} \rho(t|\, X, X)\,\mathrm{d}X \,=\, \int_{\mathbb{R}^d} R(t|\, x, 0)\,\mathrm{d}x \,=\, 1\,.$$

Translating the positivity condition on $\hat{\rho}(t) \geq 0$ in terms of the function R is more difficult and we leave it aside (see however in [12] a characterization of rank-1 density operators in Weyl's variables).

On the one hand, by a simple change of variables, we first get the conservation of the L^2 norm for equation (1.3) : for each $t \in [0, +\infty)$,

$$\iint_{\mathbb{R}^{2d}} |R(t|\, x, y)|^2 \, \mathrm{d}x \, \mathrm{d}y \;=\; \|R_\hbar^{in}\|_{L^2}^2 \;<\; \infty \,.$$

This latter property is crucial in the stability analysis of a numerical method [10].

Finally, let us point out that the von Neumann equation written in Weyl's variables (1.3) is well adapted to making the link with other formulations, such as the Wigner equation. Indeed, for all $(t, x) \in \mathbb{R}^+ \times \mathbb{R}^d$, we define the Wigner function $W(t, x, \cdot)$ by taking the Fourier transform of the function $R(t|\, x, \cdot)$

$$W(t, x, \xi) \;=\; \frac{1}{(2\pi)^d} \int_{\mathbb{R}^d} R(t|\, x, y)\, e^{-i\, y\cdot\xi} \, \mathrm{d}y \,.$$

The integral on the right-hand side is not absolutely converging in general (*i.e.* not a Lebesgue integral), but is the Fourier(-Plancherel) transform of an L^2 function on $\mathbb{R}^d$.

Then the function W is formally a solution of the so-called Wigner equation [17, Chapter 11]

$$\partial_t W \;+\; \xi \cdot \nabla_x W \;-\; \Theta[V]\, W \;=\; 0 \,, \tag{1.4}$$

where the operator $\Theta[V]$ is given by

$$\Theta[V] W(t, x, \xi) \;=\; \frac{i}{(2\pi)^d\, \hbar} \int_{\mathbb{R}^d} \left(V\left(x + \frac{\hbar}{2} y\right) \;-\; V\left(x - \frac{\hbar}{2} y\right) \right) W(t, x, \xi')\, e^{i\, y\cdot(\xi - \xi')} \, \mathrm{d}\xi' \, \mathrm{d}y \,.$$

The local term $\xi \cdot \nabla_x W$ is the quantum analogue of the classical transport term of the Liouville equation whereas the nonlocal term $\Theta[V]\, W$ describes the influence of the electric potential. In other words, while the classical limit of the von Neumann equation is a singular perturbation problem in the original variables, it becomes a regular perturbation problem for smooth potentials, when written in Weyl's variables, or for the Wigner equation.

1.2. **Semi-classical limit.** The formulation of the von Neumann equation using Weyl's variables facilitates the semi-classical limit. Indeed, passing to the limit as $\hbar \to 0$ in the latter equation does not lead to any difficulty related to the stiffness in $\hbar$. Indeed, since $V \in \mathscr{C}^1(\mathbb{R}^d)$, we have

$$\frac{V(x + \frac{\hbar}{2}\, y) - V(x - \frac{\hbar}{2}\, y)}{\hbar} \to \nabla V(x) \cdot y \qquad \text{as } \hbar \to 0 \,.$$

Therefore, we set

$$\mathcal{E}^\hbar(x, y) \;=\; \frac{V(x + \frac{\hbar}{2}\, y) - V(x - \frac{\hbar}{2}\, y)}{\hbar} \;-\; \nabla V(x) \cdot y \,, \tag{1.5}$$

and R solves

$$\begin{cases} \partial_t R(t|\, x, y) \;=\; i \displaystyle\sum_{j=1}^{d} \partial_{x_j} \partial_{y_j} R(t|\, x, y) \;-\; i \left(\nabla V(x) \cdot y \;+\; \mathcal{E}^\hbar(x, y) \right) R(t|\, x, y) \,, \\ R(0) \;=\; R_\hbar^{in} \,, \end{cases}$$

where $\mathcal{E}^\hbar$ tends to zero as $\hbar \to 0$. The error made in approximating the solution $R(t|\, x, y)$ of (1.3) by $\hat{R}(t|\, x, y)$ is analyzed in Theorem 1.1 below. The solution obtained by neglecting the source

term $\mathcal{E}^\hbar$ corresponds to the semi-classical limit, given by

$$\left\{ \begin{array}{l} \partial_t \hat{R}(t|\, x,y) \,=\, i \displaystyle\sum_{j=1}^{d} \partial_{x_j}\partial_{y_j} \hat{R}(t|\, x,y) \,-\, i\, \nabla V(x)\cdot y\, \hat{R}(t|\, x,y)\,, \\ \hat{R}(0) \,=\, \hat{R}^{in}_\hbar\,. \end{array} \right. \tag{1.6}$$

Equation (1.6) can be interpreted using the Wigner function $\widehat{W}(t,x,.)$ computed from $\hat{R}(t|\, x,\cdot)$

$$\widehat{W}(t,x,\xi) \,=\, \frac{1}{(2\pi)^d} \int_{\mathbb{R}^d} \hat{R}(t|\, x,\xi)\, e^{-i\, y\cdot\xi}\, \mathrm{d}y\,.$$

Taking the Fourier transform with respect to the y variable in (1.6), we see that the function $\widehat{W}$ solves the Liouville equation

$$\partial_t \widehat{W} \,+\, \xi\cdot\nabla_x \widehat{W} \,-\, \nabla_x V\cdot\nabla_\xi \widehat{W} \,=\, 0\,.$$

This limit was made rigorous by P.-L. Lions and T. Paul [19], and P. Markowich and C. Ringhofer [21, 23] for smooth potentials. The limit was also performed in [24, Section 1.4] by an asymptotic expansion of $\mathcal{E}^\hbar$ in powers of $\hbar$. For references on the mathematical analysis of the Wigner equation (or the Wigner–Poisson system), we refer to the review of A. Arnold [1].

In the following, we restrict ourselves to the one-dimensional case $d = 1$. Let us fix an integer $m \geq 0$ and suppose that the potential V is such that

$$V \in \mathscr{C}^{m+1}(\mathbb{R}) \quad \text{with} \quad m \geq 1 \quad \text{and} \quad V(x) \to +\infty, \quad \text{as} \quad |x| \to \infty\,, \tag{1.7}$$

and for all $n = 2, \ldots, m+1$, there exists a constant $C > 0$, not depending on $\hbar$, such that

$$\|V^{(n)}\|_{L^\infty} \leq C. \tag{1.8}$$

From this assumption we get our first result on error estimates with respect to $\hbar$ between the solution R of the von Neumann equation (1.3) and $\hat{R}$ of its classical limit (1.6).

Theorem 1.1. *Assume that V satisfies (1.7)-(1.8) with $m = 3$ while for all integers a, b, α and β such that $a + b + \alpha + \beta \leq 3$, we suppose that both initial data $R^{in}_\hbar$ and $\hat{R}^{in}_\hbar$ are such that*

$$\left\{ \begin{array}{l} \|x^a \partial_x^b y^\alpha \partial_y^\beta \hat{R}^{in}_\hbar\|_{L^2} \,<\, \mathcal{C}_0\,, \\ \|R^{in}_\hbar\|_{L^2} \,<\, \mathcal{C}_0\,, \end{array} \right. \tag{1.9}$$

where $\mathcal{C}_0 > 0$ does not depend on $\hbar$ and $L^2 = L^2_{xy} := L^2(\mathbb{R}^2)$. Then the solution R to the von Neumann equation (1.3) and the solution $\hat{R}$ to (1.6) with the initial data $R^{in}_\hbar$ and $\hat{R}^{in}_\hbar$ satisfy

$$\|R(t) \,-\, \hat{R}(t)\|_{L^2} \,\leq\, \|R^{in}_\hbar \,-\, \hat{R}^{in}_\hbar\|_{L^2} \,+\, \mathcal{C}_t\, \hbar^2 \qquad t \geq 0\,,$$

where $\mathcal{C}_t$ is a constant independent of $\hbar$.

The proof of this theorem is presented in [10] and is a simple consequence of the regularity of the solution to the semi-classical limit problem (1.6).

Remark 1.2. *Let us make the following comments on Theorem 1.1:*

- *of course, assumptions (1.9) are not the most general setting for the semi-classical limit, in particular they exclude pure WKB states;*
- *from (1.9), we know that $(\hat{R}^{in}_\hbar)_{\hbar>0}$ is strongly compact in L^2, but allows fast oscillations in $\rho(t|\, X,Y)$ in the original variables. Indeed, for a given $(\tilde{x},\tilde{p}) \in \mathbb{R}^2$, let us remind that if $(t,X) \mapsto \Psi(t,X,\tilde{x},\tilde{p})$ is a solution to the Schrödinger equation,*

$$i\,\hbar\,\partial_t \Psi \,=\, H\Psi\,,$$

then, for a given weight function K, we may define the density matrix with integral kernel

$$\rho(t|\, X, Y) = \int_{\mathbb{R}^2} K(\tilde{x},\tilde{p})\, \Psi(t, X, \tilde{x}, \tilde{p})\, \overline{\Psi}(t, Y, \tilde{x}, \tilde{p})\, \mathrm{d}\tilde{x}\, \mathrm{d}\tilde{p}\,,$$

which is a solution to the von Neumann equation (1.1). Therefore in our framework, we may consider mixed sates obtained by first choosing the WKB initial condition centered at $\tilde{x} \in \mathbb{R}$ and with an initial energy $H(\tilde{x}, \tilde{p})$,

$$\Psi^{in}(X, \tilde{x}, \tilde{p}) \;=\; \frac{1}{\sqrt{2\pi}}\, \exp\left(-\frac{|X-\tilde{x}|^2}{4}\right) \exp\left(-i\,\frac{\tilde{p}\,X}{\hbar}\right)$$

and a weight function K given by

$$K(\tilde{x}, \tilde{p}) \;=\; \frac{1}{\sqrt{s_\hbar}}\, \exp\left(-\frac{|\tilde{p}-p_0|^2}{2s_\hbar}\right)\, \delta(\tilde{x}-x_0),$$

where $s_\hbar = 1-\hbar^2/4$. Then, we construct the density function ρ^{in} as

$$\begin{aligned}\rho^{in}(X,Y) \;&=\; \int_{\mathbb{R}^2} K(\tilde{x},\tilde{p})\, \Psi^{in}(X,\tilde{x},\tilde{p})\, \overline{\Psi^{in}}(Y,\tilde{x},\tilde{p})\, \mathrm{d}\tilde{x}\, \mathrm{d}\tilde{p}\,,\\ &=\; \frac{1}{\sqrt{2\pi}}\, \exp\left(-\frac{\left(\frac{1}{2}(X+Y)-x_0\right)^2}{2} - \frac{(X-Y)^2}{2\hbar^2} - \frac{i\,p_0\,(X-Y)}{\hbar}\right),\end{aligned}$$

that is,

$$R^{in}(x,y) \;=\; \frac{1}{\sqrt{2\pi}}\, \exp\left(-\frac{|x-x_0|^2+y^2}{2} - i\,p_0 y\right).$$

In Section 4, we will consider such initial conditions.

2. Hermite spectral method

The purpose of this section is to present a formulation of the von Neumann equation (1.3) written in Weyl's variables based on Hermite polynomials. We first use Hermite polynomials in the y variable and write the von Neumann equation (1.3) as an infinite hyperbolic system for the Hermite coefficients depending only on time and on the space variable x. The idea is to apply a Galerkin method keeping only a small finite set of orthogonal polynomials rather than discretizing the operator R in y on a grid. The merit of using an orthogonal basis like the so-called scaled Hermite basis has been shown in [15, 28] and more recently in [11, 4, 5, 8, 7, 6] for the Vlasov-Poisson system. We define a weight function ω as

$$\omega(y) := \pi^{-1/4}\, e^{-y^2/2}\,, \qquad y \in \mathbb{R}\,,$$

and the sequence of Hermite polynomials (called the "physicist's Hermite polynomials"),

$$H_k(y) \;=\; (-1)^k\, \omega^{-2}(y)\, \partial_y^k \omega^2(y)\,, \qquad k \geq 0\,. \tag{2.1}$$

In this context the family of Hermite functions $(\Phi_k)_{k\in\mathbb{N}}$ defined as

$$\Phi_k(y) \;=\; \frac{1}{\sqrt{2^k k!}}\, \omega(y)\, H_k(y)\,, \qquad k \geq 0$$

is a complete, orthonormal system for the classical L^2 inner product, that is,

$$\int_{\mathbb{R}} \Phi_k(y)\, \Phi_l(y)\, \mathrm{d}y \;=\; \delta_{k,l}\,, \quad \text{and} \quad \overline{\mathrm{Span}\{\Phi_k, \quad k\geq 0\}} = L^2(\mathbb{R}).$$

Moreover, the sequence $(H_k)_{k\in\mathbb{N}}$ defined in (2.1) satisfies the recursion relation,

$$\begin{cases} H_{-1} = 0, \quad H_0 = 1, \\ H_{k+1}(y) \,=\, 2\,y\,H_k(y) \,-\, 2\,k\,H_{k-1}(y)\,, \quad k \,\geq\, 0\,. \end{cases}$$

Let us also point out that the Hermite functions also verify the following relations

$$\Phi_k'(y) \,=\, -\sqrt{\frac{k+1}{2}}\,\Phi_{k+1}(y) \,+\, \sqrt{\frac{k}{2}}\,\Phi_{k-1}(y)\,, \quad \forall\, k \,\geq\, 0\,, \tag{2.2}$$

and

$$y\,\Phi_k(y) \,=\, \sqrt{\frac{k+1}{2}}\,\Phi_{k+1}(y) \,+\, \sqrt{\frac{k}{2}}\,\Phi_{k-1}(y)\,, \quad \forall\, k \,\geq\, 0\,. \tag{2.3}$$

We now set for any $N \geq 0$,

$$\mathscr{P}_N(\mathbb{R}) \,=\, \mathrm{Span}\{\Phi_k, \quad k = 0, \dots, N\}\,,$$

and expand the solution to the von Neumann and semi-classical limit equations (1.3) and (1.6) in terms of Hermite functions in the variable y.

2.1. **Hermite approximation of the von Neumann equation.** We consider the decomposition of R, solution to (1.3), into its components $R \,=\, (R_k)_{k\in\mathbb{N}}$ in the Hermite basis:

$$R\,(t|\,x,y) \,=\, \sum_{k\in\mathbb{N}} R_k\,(t|\,x)\;\Phi_k(y)\,,$$

where

$$R_k(t|\,x) \,:=\, \int_{\mathbb{R}} R(t|\,x,y)\,\Phi_k(y)\,\mathrm{d}y\,, \quad k \geq 0\,.$$

Using the recursion relations (2.2)-(2.3), for all $k \geq 0$,

$$\begin{aligned} \int_{\mathbb{R}} \partial_y R(t|\,x,y)\,\Phi_k(y)\,\mathrm{d}y \;&=\; -\int_{\mathbb{R}} R(t|\,x,y)\,\partial_y\Phi_k(y)\,\mathrm{d}y \\ &=\; -\sqrt{\frac{k}{2}}\,R_{k-1}(t|\,x) \,+\, \sqrt{\frac{k+1}{2}}\,R_{k+1}(t|\,x)\,, \end{aligned}$$

with $R_{-1} = 0$, whereas

$$\int_{\mathbb{R}} R(t|\,x,y)\,y\,\Phi_k(y)\,\mathrm{d}y \;=\; \sqrt{\frac{k}{2}}\,R_{k-1}(t|\,x) \,+\, \sqrt{\frac{k+1}{2}}\,R_{k+1}(t|\,x)\,.$$

Similarly,

$$\int_{\mathbb{R}} \left\{ \frac{V(x+\frac{\hbar}{2}\,y) - V(x-\frac{\hbar}{2}\,y)}{\hbar} - V'(x)\,y \right\} R(t|\,x,y)\Phi_k(y)\,\mathrm{d}y \,=\, \sum_{l\in\mathbb{N}} \mathcal{E}^\hbar_{k,l}(x)\,R_l(t|\,x)\,,$$

with

$$\mathcal{E}^\hbar_{k,l}(x\,) := \int_{\mathbb{R}} \mathcal{E}^\hbar(x,y)\,\Phi_k(y)\Phi_l(y)\,\mathrm{d}y\,, \qquad k,\,l \,\in\, \mathbb{N}\,, \tag{2.4}$$

where the function $\mathcal{E}^\hbar(.,.)$ is defined in (1.5).

Let us first review some properties of $\mathcal{E}_{k,l}$. Obviously $\mathcal{E}^\hbar_{k,l}(x) \in \mathbb{R}$ and

$$\mathcal{E}_{k,l}(x) \,=\, \mathcal{E}_{l,k}(x)\,, \qquad x \in \mathbb{R},\; k,l \geq 0\,.$$

Furthermore, applying the change of variable $y \mapsto -y$ in (2.4) and using that $H_k(y) = (-1)^k H_k(-y)$ we also get

$$\mathcal{E}^\hbar_{k,l}(x) = -(-1)^{k+l}\,\mathcal{E}^\hbar_{k,l}(x)\,, \qquad x \in \mathbb{R},\, k,l \geq 0\,.$$

This latter property implies that $\mathcal{E}^\hbar_{k,l}$ is identically 0 whenever $k+l$ is even.

We thus end up with the formulation of the von Neumann equation (1.3) written in the Hermite basis in y for all $k \geq 0$,

$$\begin{cases} \partial_t R_k + i\left(\sqrt{\frac{k}{2}}\,\mathcal{D}\,R_{k-1} + \sqrt{\frac{k+1}{2}}\,\mathcal{D}^\star R_{k+1}\right) = -i\sum_{l\in\mathbb{N}} \mathcal{E}^\hbar_{k,l}\,R_l\,, \\ R_k(t=0) = R^{in}_{\hbar,k}\,, \end{cases}$$

where $\mathcal{D}$ and $\mathcal{D}^\star$ are given by

$$\begin{cases} \mathcal{D}\,u &= +\partial_x u + V'(x)\,u\,, \\ \mathcal{D}^\star\,u &= -\partial_x u + V'(x)\,u\,. \end{cases}$$

Let us emphasize an important property satisfied by $\mathcal{D}$, which we will need to recover later on, in the discrete setting. The operator $\mathcal{D}^\star$ is its adjoint operator in $L^2(\mathbb{R})$, so that for all u, $v \in \mathrm{Dom}(\mathcal{D})$ it holds

$$\langle \mathcal{D}^\star u,\, v\rangle = \langle u,\, \mathcal{D}v\rangle\,, \tag{2.5}$$

where $\langle .,\, .\rangle$ denotes the $L^2(\mathbb{R}^d)$ inner product. Then we define an approximation $R^N = (R^N_k)_{0\leq k\leq N} \in \mathscr{P}_N(\mathbb{R})$ solution to the following system obtained after neglecting Hermite modes of order larger than N, that is, for $0 \leq k \leq N$

$$\begin{cases} \partial_t R^N_k + i\left(\sqrt{\frac{k}{2}}\,\mathcal{D}R^N_{k-1} + \sqrt{\frac{k+1}{2}}\,\mathcal{D}^\star R^N_{k+1}\right) = -i\sum_{l=0}^{N} \mathcal{E}^\hbar_{k,l}\,R^N_l\,, \\ R^N_k(0) = R^{in}_{\hbar,k}\,, \end{cases} \tag{2.6}$$

where $R^N_{-1} = R^N_{N+1} = 0$.

2.2. **Review of error estimates.** Here we suppose that for a fixed $m \geq 0$ and for all integer a, b, α and β such that $a+b+\alpha+\beta \leq m$, we have

$$\|x^a \partial_x^b y^\alpha \partial_y^\beta R^{in}_\hbar\|_{L^2} < \infty. \tag{2.7}$$

In [10], we have obtained error estimates between the Hermite-Galerkin approximation and the solution to the von Neumann equation (1.3). As we have seen before, the formulation (2.6) is well adapted to obtaining the semi-classical limit as $\hbar \to 0$. Indeed, the Hermite formulation of the semi-classical limit equation (1.6) is obtained simply by neglecting the right-hand side term in (2.6). Thus, $\hat{R}^N = (\hat{R}^N_k)_{0\leq k\leq N}$ satisfies, for all $k \in \{0,\dots,N\}$,

$$\begin{cases} \partial_t \hat{R}^N_k + i\left(\sqrt{\frac{k}{2}}\,\mathcal{D}\hat{R}^N_{k-1} + \sqrt{\frac{k+1}{2}}\,\mathcal{D}^\star \hat{R}^N_{k+1}\right) = 0\,, \\ \hat{R}^N_k(t=0) = \hat{R}^{in}_{\hbar,k}\,. \end{cases} \tag{2.8}$$

Moreover, under regularity assumption on the initial data, we prove error estimates of the Hermite-Galerkin method for smooth solutions of the semi-classical limit equation (1.6).

For a given $m \geq 0$ and for all integer a, b, α and β such that $a+b+\alpha+\beta \leq m$, we suppose that the initial data $\hat{R}^{in}_\hbar$ satisfies

$$\|x^a \partial_x^b y^\alpha \partial_y^\beta \hat{R}^{in}_\hbar\|_{L^2} < \infty. \tag{2.9}$$

Thus, the error estimates, proven in [10], can be summarized in the following theorem.

Theorem 2.1. *Let $p \geq 1$ and assume that V satisfies (1.7)-(1.8) with $m = 2(p+1)$ while for all integers a, b, α and β such that $a+b+\alpha+\beta \leq 2(p+1)$. Then we have the following result :*

- *under the assumption (2.7) on the initial data, the solutions R to (1.3) and R^N to (2.6) satisfy*

$$\|R^N(t) - R(t)\|_{L^2} \quad \leq \quad \frac{\mathcal{C}_t}{(2N+3)^{p-1/2}} \left(1+\hbar^2\right) ,$$

- *under the assumption (2.9) on the initial data, the solutions $\hat{R}$ to (1.6) and $\hat{R}^N$ to (2.8) satisfy*

$$\|\hat{R}(t) \; - \; \hat{R}^N(t)\|_{L^2} \; \leq \; \frac{\mathcal{C}_t}{(2N+3)^{p-1/2}} ,$$

where $\mathcal{C}_t$ is a constant depending only on p, V and the initial data.

The key point in the proof of Theorem 2.1 is to establish some regularity estimates on the solution to the von Neumann equation written in Weyl's variables

3. Finite volume in x and time discretization

This section is devoted to the discretization of the space variable x and the time discretization. The aim is to preserve, at the discrete level, the properties of the operators $\mathcal{D}$ and $\mathcal{D}^\star$ in (2.6) and (2.8), and the conservation of the L^2 norm for both equations. Furthermore, in order to reduce the computational cost, we also propose an approximation of the non-local term $\mathcal{E}^\hbar$ by only keeping only the second order term with respect to $\hbar$. This latter approximation is valid only when $\hbar \ll 1$.

3.1. Finite volume method.

We first treat the discretization with respect to the space variable x, providing an approximation of the operators $\mathcal{D}$ and $\mathcal{D}^\star$. In order to get L^2 stability on the numerical solution, we aim at preserving the duality structure (2.5) of the discrete operators.

We fix a number of Hermite modes $N \in \mathbb{N}^*$ and consider an interval (a,b) of $\mathbb{R}$. For $N_x \in \mathbb{N}^\star$, we introduce the set $\mathcal{J} = \{1, \ldots, N_x\}$, and a family of control volumes $(K_j)_{j\in\mathcal{J}}$ such that $K_j = (x_{j-1/2}, x_{j+1/2})$, where x_j is the midpoint of the interval K_j, *i.e.* $x_j = (x_{j-1/2}, x_{j+1/2})/2$, and

$$a = x_{1/2} < x_1 < x_{3/2} < \ldots < x_{j-1/2} < x_j < x_{j+1/2} < \ldots < x_{N_x} < x_{N_x+1/2} = b \, .$$

Let us introduce the mesh size

$$\Delta x \; = \; x_{j+1/2} - x_{j-1/2} \, ,$$

and $\delta = (N, \Delta x)$ the numerical parameter. Then we denote by $R_k^\delta(t) = (\mathcal{R}_{k,j}(t))_{j\in\mathcal{J}}$, for $k \in \{0, \ldots, N\}$, the approximation of $R_k^N(t)$, where the index k represents the k-th mode of the Hermite decomposition, whereas $\mathcal{R}_{k,j}(t)$ is an approximation of the mean value of $R_k(t)$ over the cell K_j at time t.

First of all, the initial condition is discretized on each cell K_j by:

$$\mathcal{R}_{k,j}(0) \; = \; \frac{1}{\Delta x} \int_{K_j} R_k^N(t=0,x) \, \mathrm{d}x, \quad j \in \mathcal{J} \, .$$

By integrating equation (2.6) on K_j for $j \in \mathcal{J}$, we obtain the following numerical scheme :

$$\frac{\mathrm{d}R_k^\delta}{\mathrm{d}t} + i \left(\sqrt{\frac{k}{2}} \, \mathcal{D}_{\Delta x} \, R_{k-1}^\delta + \sqrt{\frac{k+1}{2}} \, \mathcal{D}_{\Delta x}^\star \, R_{k+1}^\delta \right) = -i \sum_{l=0}^{N} \mathcal{E}_{k,l}^\hbar \, R_l^\delta \, , \tag{3.1}$$

where $\mathcal{D}_{\Delta x}$ (resp. $\mathcal{D}_{\Delta x}^\star$) is an approximation of the operator $\mathcal{D}$ (resp. $\mathcal{D}^\star$) given by

$$\mathcal{D}_{\Delta x} = (\mathcal{D}_j)_{j\in\mathcal{J}} \quad \text{and} \quad \mathcal{D}_{\Delta x}^\star = (\mathcal{D}_j^\star)_{j\in\mathcal{J}}$$

and where for $R^\delta = (\mathcal{R}_j)_{j\in\mathcal{J}}$ it holds

$$\left\{\begin{array}{rcl} \mathcal{D}_j R^\delta &=& +\dfrac{\mathcal{R}_{j+1}-\mathcal{R}_{j-1}}{2\Delta x} - E_j\,\mathcal{R}_j\,, \quad j\in\mathcal{J}\,,\\[2ex] \mathcal{D}_j^\star R^\delta &=& -\dfrac{\mathcal{R}_{j+1}-\mathcal{R}_{j-1}}{2\Delta x} - E_j\,\mathcal{R}_j\,, \quad j\in\mathcal{J}\,. \end{array}\right. \tag{3.2}$$

On the other hand, the discrete force field E_j is computed in terms of the applied potential V as

$$E_j \;=\; -\frac{V(x_{j+1})-V(x_{j-1})}{2\Delta x}\,. \tag{3.3}$$

It is worth mentioning that the same kind of approximation has been successfully applied to the Vlasov-Poisson and Vlasov-Poisson-Fokker-Planck systems. It allows to preserve the structure of the continuous equation [8, 7, 6], which is particularly convenient to capture the long time dynamics. Finally we apply a Crank-Nicolson scheme for the time discretization with a time step Δt.

3.2. **Approximation of the non-local term when $\hbar \ll 1$.** Let us emphasize that the evaluation of the right-hand side $\left(\mathcal{E}_{k,l}^\hbar\right)_{0\le k,\,l\le N}$ in (3.1) may be costly since the computational complexity of each time step is of order $N^2\,N_x$. However, using the smoothness of the potential V and the fact that $\hbar \ll 1$, the non local term can be drastically simplified. Indeed, let us suppose that the potential V is real and analytic on $\mathbb{R}$, so that

$$V(z\,) = \sum_{n\ge 0}\frac{1}{n!}\,V^{(n)}(x)\,(z-x)^n\,,$$

hence we have

$$\frac{V(x+\frac{1}{2}\hbar y)-V(x-\frac{1}{2}\hbar y)}{\hbar} \;=\; \sum_{n\ge 0}\frac{\hbar^{2n}}{2^{2n}\,(2n+1)!}V^{(2n+1)}(x)\,y^{2n+1}\,,$$

and

$$\mathcal{E}_{k,l}^\hbar(x) = \sum_{n\ge 1}\frac{\hbar^{2n}}{2^{2n}(2n+1)!}V^{(2n+1)}(x)\int_{\mathbb{R}} y^{2n+1}\,\Phi_k(y)\,\Phi_l(y)\,\mathrm{d}y\,.$$

Applying twice the recursion relation (2.2) shows that

$$y^2\Phi_k(y) \;=\; \frac{\sqrt{k(k-1)}}{2}\,\Phi_{k-2}(y) \;+\; \frac{2k+1}{2}\,\Phi_k(y) \;+\; \frac{\sqrt{(k+1)(k+2)}}{2}\,\Phi_{k+2}(y)\,,$$

Using again (2.2) and the L^2-orthogonality of the Hermite functions, we find that

$$\begin{array}{rcl} \displaystyle\int_{\mathbb{R}} y^3\,\Phi_k(y)\,\Phi_l(y)\,\mathrm{d}y &=& \sqrt{\dfrac{k(k-1)^2}{8}}\delta_{k,l+1} + \dfrac{2k+1}{2}\sqrt{\dfrac{k+1}{2}}\delta_{k,l-1}\\[2ex] &+& \sqrt{\dfrac{(k+1)(k+2)(k+3)}{8}}\delta_{k,l-3} + \sqrt{\dfrac{k(k-1)(k-2)}{8}}\delta_{k,l+3}\\[2ex] &+& \dfrac{2k+1}{2}\sqrt{\dfrac{k}{2}}\delta_{k,l+1} + \sqrt{\dfrac{(k+1)(k+2)^2}{8}}\delta_{k,l-1}\,. \end{array}$$

Combining with the former Hermite-Galerkin method, we get for $0 \leq k \leq N$,

$$
\begin{cases}
\dfrac{\mathrm{d}R_k^\delta}{\mathrm{d}t} \,+\, i\,\left(\sqrt{\dfrac{k}{2}}\mathcal{D}_{\Delta x}R_{k-1}^\delta \,+\, \sqrt{\dfrac{k+1}{2}}\mathcal{D}_{\Delta x}^\star R_{k+1}^\delta\right) \,=\, -\,i\,\hbar^2\,\mathcal{S}_k[R^\delta]\,, \\[2ex]
\mathcal{S}_k[R^\delta] \,=\, \dfrac{V^{(3)}}{24}\,\left(\dfrac{3}{2}\,k\,\sqrt{\dfrac{k}{2}}\,R_{k-1}^\delta \,+\, \dfrac{3}{2}\,(k+1)\,\sqrt{\dfrac{k+1}{2}}\,R_{k+1}^\delta\right. \\[2ex]
\qquad\qquad \left. +\,\sqrt{\dfrac{k(k-1)(k-2)}{8}}\,R_{k-3}^\delta \,+\, \sqrt{\dfrac{(k+1)(k+2)(k+3)}{8}}\,R_{k+3}^\delta\right),
\end{cases}
\tag{3.4}
$$

where $V^{(3)}(x)$ is an approximation of the third order derivative of the potential V.

This approximation of the source term introduces an additional error of order $\hbar^4$, which means that this latter approximation is valid only when $\hbar$ is small compared to $1/N$, where N is the number of Hermite modes, Δx the mesh size and Δt the time time.

4. Numerical simulations

In the following we perform several numerical simulations to illustrate the efficiency of the proposed Finite Volume/ Hermite Spectral method for the approximation of the solution to the von Neumann equation (1.3) for various potentials V. We will for instance consider smooth potential with strong confining properties.

4.1. **Harmonic potential.**

We first consider the isotropic harmonic potential

$$V(x) = \frac{x^2}{2}$$

in order to benchmark the convergence rate of the proposed method. Indeed, the von Neumann equation (1.3) with this potential has explicit solutions, which can be used as references to validate numerical results. In this situation, the Wigner equation (1.4) on W reduces to the transport equation in phase-space

$$\partial_t W \,+\, \xi\partial_x W \,-\, \partial_x V\,\partial_\xi W \,=\, 0\,.$$

The exact solution is $W(t,x,\xi) = W_0(x(t),\xi(t))$, where

$$
\begin{cases}
x(t) \,=\, \cos(t)\,x(0) \,-\, \sin(t)\,\xi(0)\,, \\
\xi(t) \,=\, \sin(t)\,x(0) \,+\, \cos(t)\,\xi(0)\,.
\end{cases}
$$

Consider a Gaussian wavepacket

$$W^{in}(x,\xi) \,=\, \frac{1}{2\pi}\,\exp\left(-\frac{(x-5)^2+\xi^2}{2}\right)$$

as initial condition, so that the wavepacket returns to the initial state at the final time $T = 2\pi$. It is worth mentioning that our Hermite spectral method is well suited to compute the Wigner transform. Indeed, W corresponds to the Fourier transform of R and Hermite functions Φ_k are eigenfunctions of the Fourier transform :

$$\mathcal{F}(\Phi_k)(\xi) \,=\, (-i)^k\,\Phi_k(\xi),$$

where $\mathcal{F}$ represents the Fourier transform.

$(\Delta t,\, \Delta x)$	L^2 numerical error	Order
0.640	0.21458	X
0.320	0.10280	1.06
0.160	0.02930	1.82
0.080	0.00766	1.94
0.040	0.00191	2.00

(a) $N = 20$

$(\Delta t,\, \Delta x)$	L^2 numerical error	Order
0.640	0.22687	X
0.320	0.10379	1.13
0.160	0.02931	1.81
0.080	0.00736	1.99
0.040	0.00184	2.00

(b) $N = 200$

TABLE 4.1. **Harmonic potential :** L^2 error with respect to $(\Delta t, \Delta x)$ and the number of Hermite modes N.

Here, we choose the x domain as $[-8, 8]$ and mainly focus on the convergence with respect to Δx, $1/N$, and the time step Δt. Numerical errors are presented in Table 4.1, where the numerical error is given as

$$\mathcal{E}(\Delta t, \Delta x) \;=\; \max_{n\geq 0} \left(\sum_{k=0}^{N} \sum_{j=0}^{N_x} \Delta x \, |\mathcal{R}^n_{k,j} - R_k(t^n, x_j)|^2 \right)^{1/2} .$$

From the results, we can make the following observations. On the one hand, we present two tables showing the numerical error for $N = 20$ and $N = 200$. For this choice of the initial data, few Hermite modes may be used and the numerical error due to the truncation N is negligible. On the other hand, the convergence rate is plotted in the third column of each table. One can achieve second order convergence in Δx and Δt, according with the theoretical value of the centred finite volume scheme in x and Crank-Nicolson time discretization.

Finally in Figure 4.1, we present several snapshots of the Wigner function in phase space $x - \xi$ with $N = 20$ and $\Delta x = 0.04$.

4.2. **Quantum revivals.** The quantum revival is a fascinating phenomenon in quantum mechanics that involves periodic recurrences of the quantum wave function to its original form during time evolution. These recurrences may occur multiple times in space, leading to the formation of fractional revivals, or they may occur almost exactly to the wave function's original state at the beginning, also known as full revivals [20].

To observe this phenomenon, we now use the following quartic potential:

$$V(x) = \frac{x^2}{2} \;+\; \frac{\beta\, x^4}{4},$$

with $\beta = 0.5$. By injecting this potential in the von Neumann equation (1.3), one can easily verify that the von Neumann equation takes the simple form:

$$\partial_t R \;=\; i \left(\partial_{xy} R \;-\; V'(x)\, y R \;-\; \frac{\beta\, \hbar^2}{4}\, x\, y^3 R \right)$$

since derivatives of order larger than five of the potential vanish identically. We then choose the initial datum [20]

$$R^{in}(x, y) \;=\; \frac{1}{\sqrt{2\pi}\sigma_x} \exp\left(-\frac{1}{2} \left(\frac{x^2}{\sigma_x^2} + y^2 \right) \right) ,$$

with $\sigma_x = 0.6$, which corresponds to the following Wigner distribution

$$W^{in}(x, \xi) \;=\; \frac{1}{2\pi\sigma_x} \exp\left(-\frac{1}{2} \left(\frac{x^2}{\sigma_x^2} + \xi^2 \right) \right) .$$

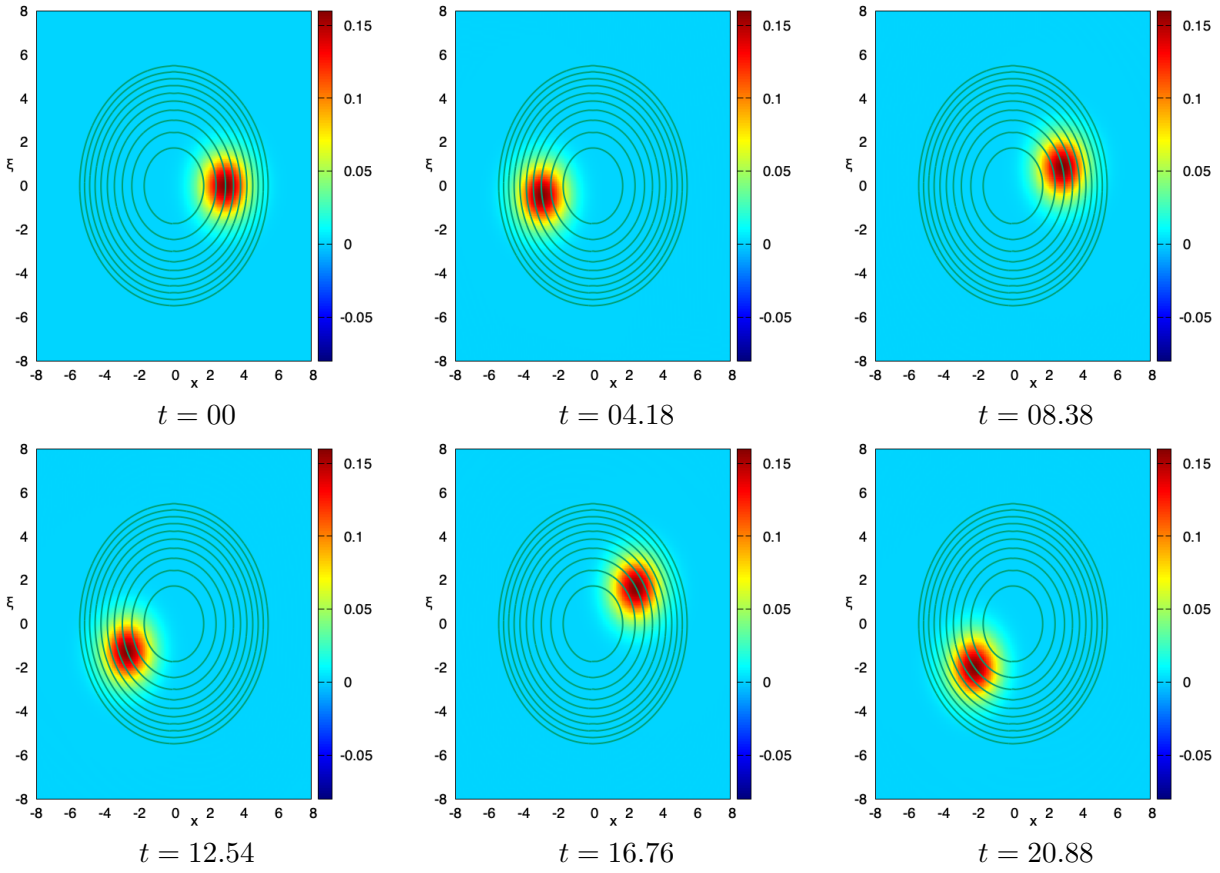

FIGURE 4.1. **Harmonic potential** : Time evolution of the Wigner function computed from the approximation of R. The lines represent the level set of the Hamiltonian $H(x,\xi) = (x^2+\xi^2)/2$.

Here, we pick the x domain to be $[-4,4]$ with $N_x = 400$, $N = 400$ and $\Delta t = 0.01$ and use the scheme (3.4), since the local approximation of $\mathcal{E}^\hbar$ is exact for such a potential.

In [20], quantum revivals, also named "quantum echoes" have been studied in the context of an anharmonic potential using the Wigner formalism, where quantum mechanics is expressed in phase space. It was found that mechanical effects prevent complete phase mixing, leading to the emergence of a linear echo. Indeed, when $\hbar$ is small, the kinetic energy relaxes to a stationary value. This is due to the phase mixing induced by the quartic term in the potential V. However, when $\hbar$ is large ($\hbar \geq 0.2$) at a subsequent time, large oscillations (the echo) appear. This phenomenon can be observed during the time evolution of the kinetic energy,

$$\mathcal{K}(t) \;=\; -\frac{1}{2}\int_{\mathbb{R}} \partial_y^2 R(t,x,0)\,\mathrm{d}x \;=\; \int_{\mathbb{R}^2} W(t,x,\xi)\,|\xi|^2\,\mathrm{d}\xi\,\mathrm{d}x\,,$$

which is represented in Figure 4.2 for different values of $\hbar = 0.01,\ 0.1,\ 0.2$ and 0.5. When $\hbar$ decreases, the echo amplitude goes to zero, while the time of its appearance is rejected to infinity. On the opposite, when $\hbar = 0.5$, the second order term with respect to $\hbar$ in the von Neumann equation becomes significant and prevents small structures in phase space from emerging. As a result, the kinetic energy maintains its oscillatory behavior (see Figure 4.2).

Figures 4.3 and 4.4 show the phase portrait for the evolution of the Wigner function starting from the Gaussian initial state W^{in}. When $\hbar$ is small ($\hbar = 0.01$), the distribution function W soon develops a spiral structure, displaying a very fine filamentation, which is the ultimate cause of the

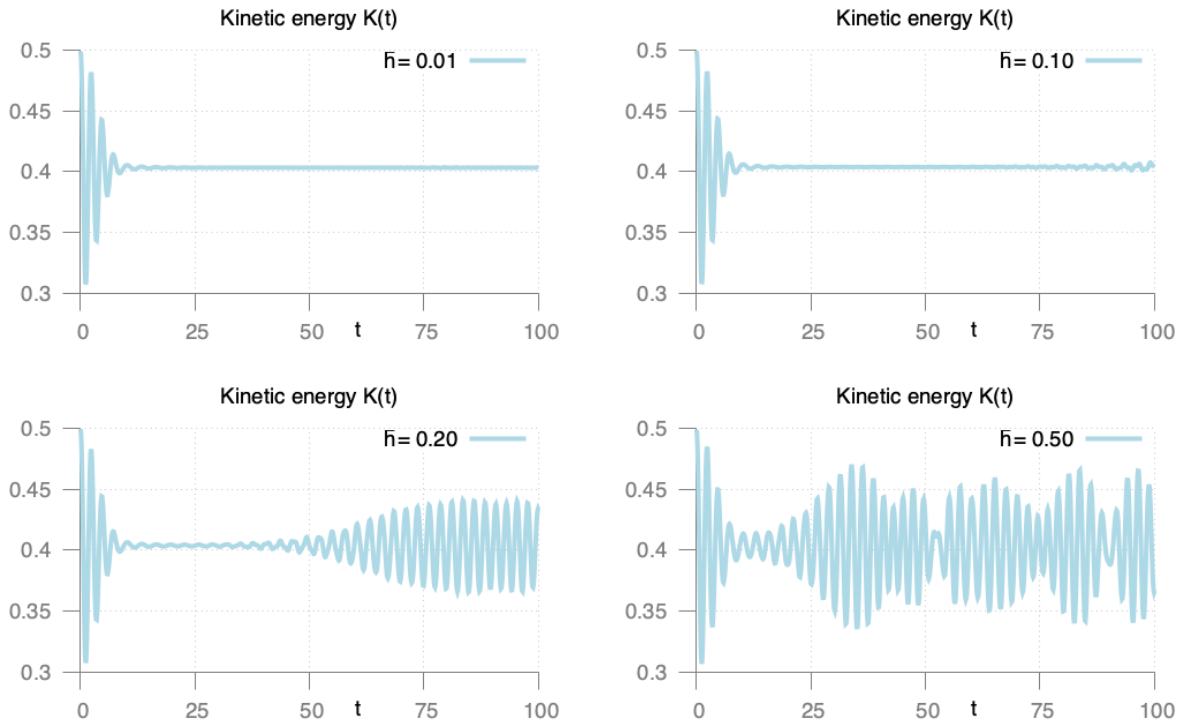

FIGURE 4.2. **Quantum revivals** : Time evolution of the kinetic energy $\mathcal{K}(t)$ for different values of $\hbar = 0.01$, $\hbar = 0.1$, $\hbar = 0.2$ and $\hbar = 0.5$.

kinetic energy relaxation. In the limit $\hbar \to 0$ this phenomena still holds. The same simulation is repeated in the quantum case when $\hbar = 0.5$ and is presented in Figure 4.4. We see that complete phase mixing is now stopped by a nonzero $\hbar$, via the second order term $\hbar^2 \beta x y^3 R/4$. The correlations among these structures are responsible for the appearance of the echo. All these numerical results are consistent with those presented in [20] on the numerical simulation of the Wigner equation. It is worth mentioning that when $\hbar \ll 1$, the quartic potential predominates and induces small structures which are persistent in the limit $\hbar \to 0$, hence both Δx and $1/N$ have to be chosen sufficiently small to follow the filamentation in phase space (see Figure 4.3) but this phenomena is not due to the fact that $\hbar > 0$!

Finally in order to illustrate again the consequence of the amplitude of $\hbar$ on the behavior of the solution, we present the macroscopic density ρ, momentum ρu and ρe, given by

$$\left\{ \begin{array}{l} \rho(t,x) \;=\; R(t,x,0)\,, \\ \rho\, u(t,x) \;=\; i\,\partial_y R(t,x,0)\,, \\ \rho\, e(t,x) \;=\; -\dfrac{1}{2}\partial_y^2 R(t,x,0)\,, \end{array} \right. \tag{4.1}$$

at time $t = 50$ for $\hbar = 0.5$ and $\hbar = 0.01$ in Figure 4.5. When $0 \leq \hbar \ll 0.01$, our numerical scheme is stable and we do not observe the influence of $\hbar$ on the solution since transport effects dominate.

While the energy density ρe remains consistent regardless of the value of $\hbar$, the densities ρ and ρu display distinct behaviors. When $\hbar$ is small, the phase space filamentation produces small oscillations in the density ρ and the momentum $\rho\, u$, while a significant oscillation is evident in the momentum for $\hbar = 0.5$.

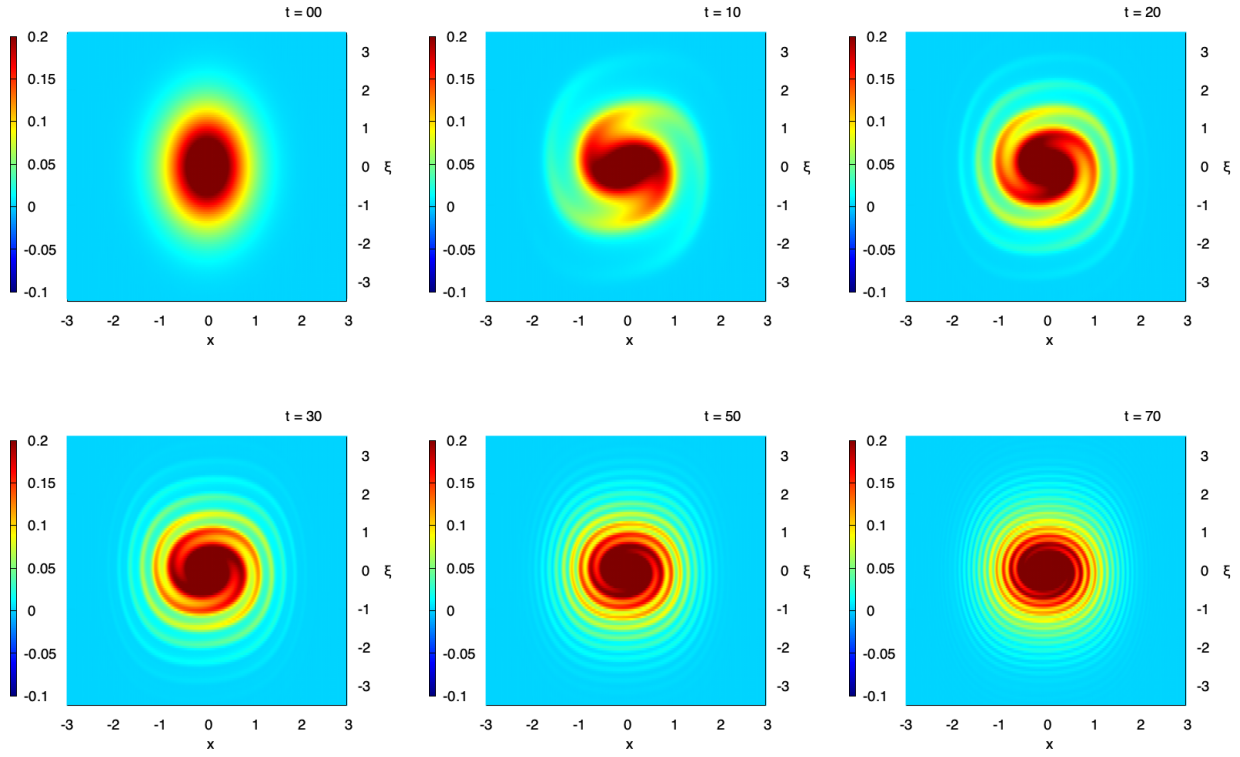

FIGURE 4.3. **Quantum revivals** : Snapshots of the Wigner distribution $W(t,x,\xi)$ at time $t = 0$, 10, 20, 30, 50 and 70 for $\hbar = 0.01$.

4.3. **Quantum tunneling.** Quantum tunneling is a phenomenon in physics where particles like electrons or atoms can pass through energy barriers that classical mechanics would deem impassable due to insufficient energy. However, in quantum mechanics, there is a probability that a particle can "tunnel" through the barrier without having the required energy. Quantum tunneling is a crucial concept in various fields, including particle physics, solid-state physics, and nuclear fusion.

Here we choose the following potential V :

$$V(x) \;=\; e^{-x^2/2}\,,$$

and the initial datum in the von Neumann equation is

$$R^{in}(x,y) \;=\; \frac{1}{\sqrt{2\pi}\sigma_x}\exp\left(-\frac{1}{2}\left(\frac{(x-x_0)^2}{\sigma_x^2}+y^2\right)\right)e^{4\,i\,y}\,,$$

with $x_0 = -5$ and $\sigma_x = 0.6$. Here, we pick the x domain to be $[-12, 16]$ with $N_x = 1000$, while $N = 400$ and $\Delta t = 0.01$.

On the one hand, we perform several numerical simulations with $\hbar = 0.1$ and even smaller values ($\hbar = 10^{-2}$, 10^{-3}) using (3.1)-(3.3) where the nonlocal term $\mathcal{E}^\hbar$ is given by (2.4) and its truncated approximation (3.4) of order $\hbar^4$. For such a configuration, both approximations give similar results and we only present those obtained with (3.1)-(3.3) and $\hbar = 0.1$ in Figures 4.6 and 4.9.

The time evolution of the Wigner function in phase space, *i. e.* in (x,ξ)-space, is proposed in Figure 4.6. The initial Gaussian beam first moves forward, then it is deviated by the strong potential as it approaches $x = 0$. Then at time $t = 1.6$, the beam goes backward but a small portion goes through the barrier created by the potential and continues its way forward. This

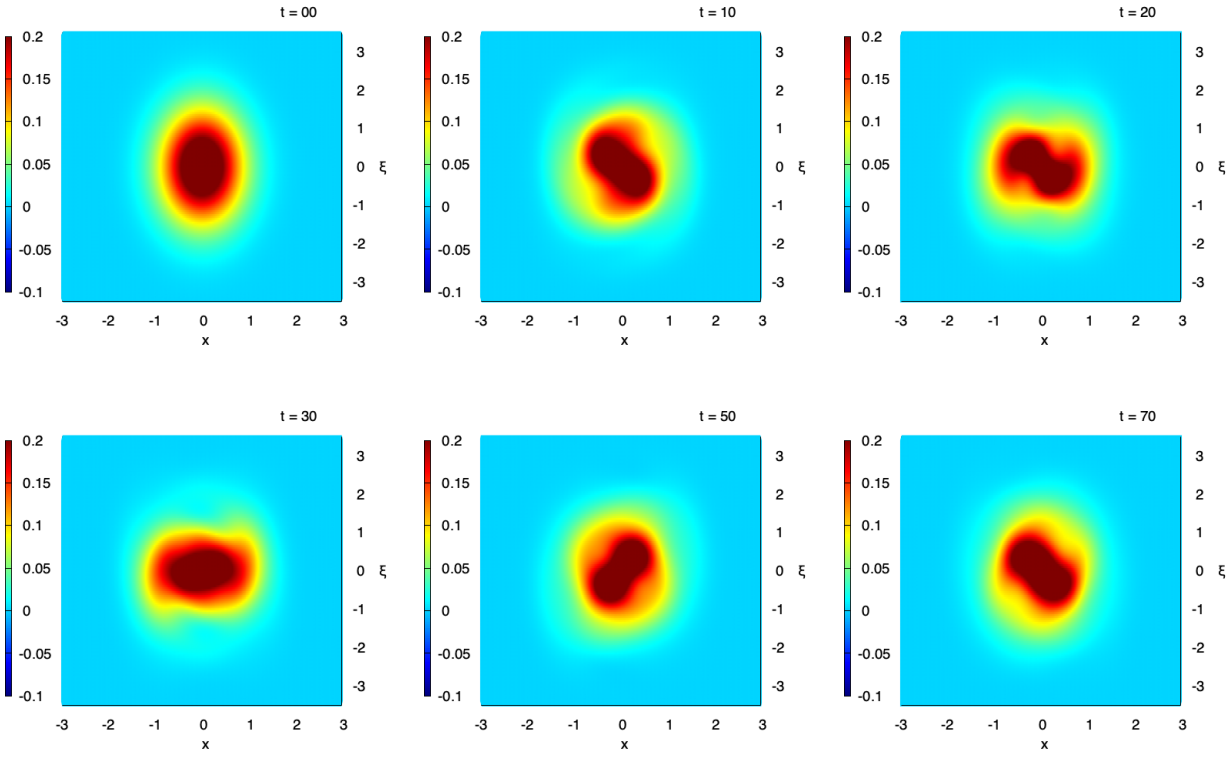

FIGURE 4.4. **Quantum revivals** : Snapshots of the Wigner distribution $W(t, x, \xi)$ at time $t = 0$, 10, 20, 30, 50 and 70 for $\hbar = 0.5$.

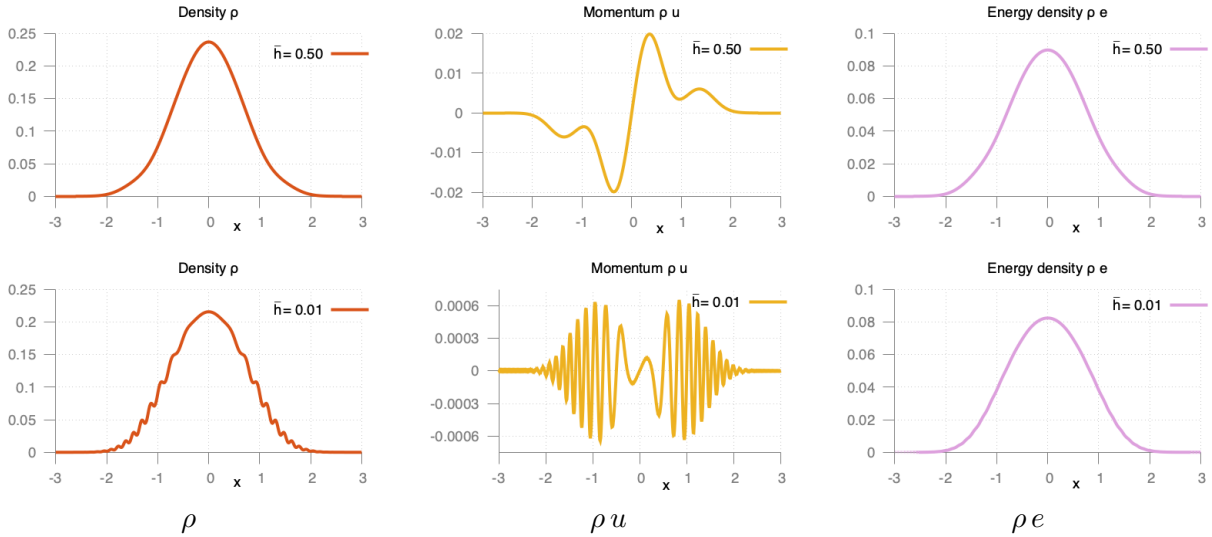

FIGURE 4.5. **Quantum revivals** : Snapshots of the matrix density $R(t, x, y)$ and the density ρ, momentum $\rho\, u$ and energy density $\rho\, e$ at time $t = 50$ for $\hbar = 0.5$ (top) and $\hbar = 0.01$ (bottom).

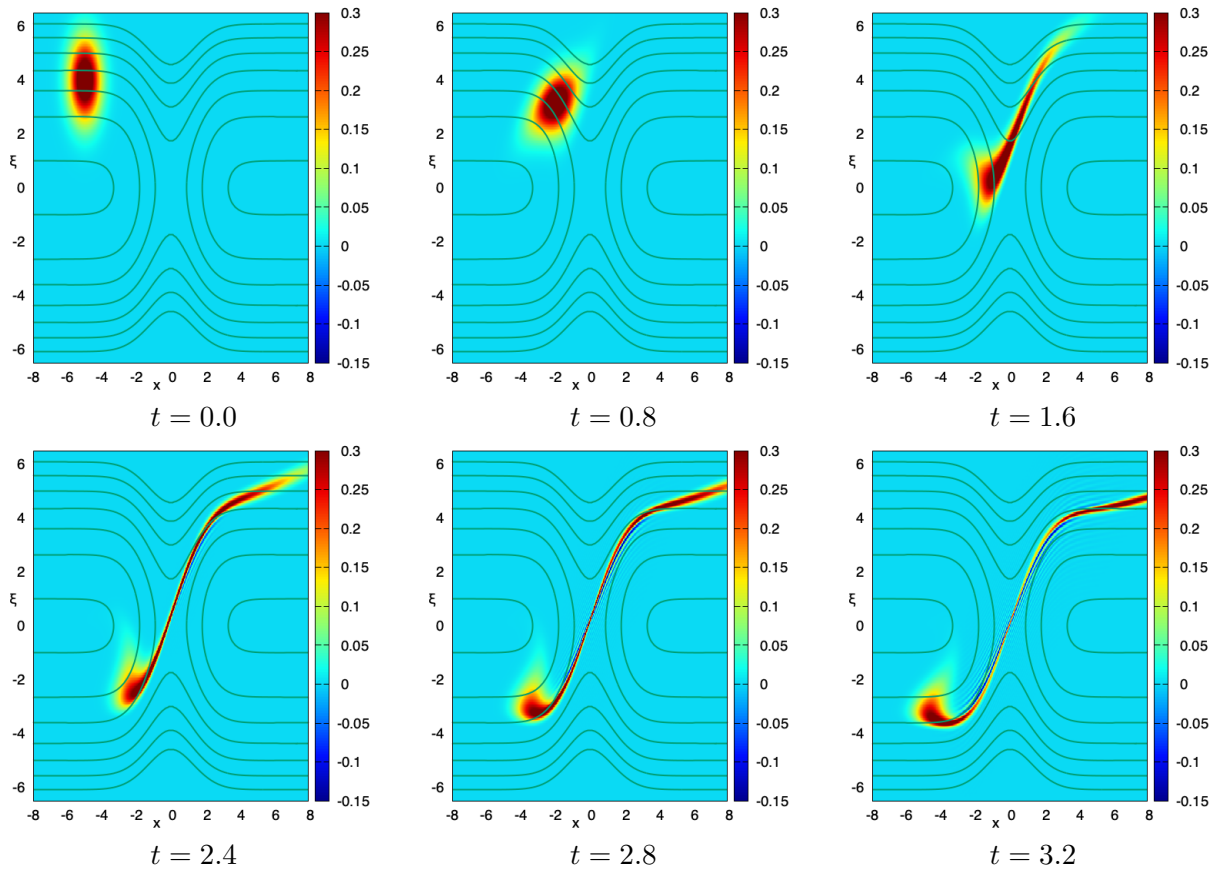

FIGURE 4.6. **Quantum tunneling** : Time evolution of the Wigner function computed from the approximation of R with $\hbar = 0.1$. The lines represent the level set of the Hamiltonian $H(x,\xi) = V(x) + \xi^2/2$.

behavior can also be observed on the macroscopic quantities ρ, $\rho\, u$ and $\rho\, e$ defined in (4.1) in Figure 4.9 when $\hbar = 0.1$. Indeed, at time $t = 1.6$ that a small amount of the density passes through the quantum barrier and moves forward. When $\hbar \ll 0.1$, we do not observe any change on the numerical approximation. Here again the use of Weyl's variables is a great advantage in the vanishing $\hbar$ limit!

On the other hand, when we increase the value of $\hbar \geq 0.5$, the local approximation of $\mathcal{E}^\hbar$ given by (2.4) is not satisfying. To illustrate this fact we present in Figure 4.10, the time evolution of the following quantities

$$\mathcal{D}_2^\hbar(t) \;=\; \left\| \left(\frac{V\left(x + \frac{\hbar}{2}\, y\right) \;-\; V\left(x - \frac{\hbar}{2}\, y\right)}{\hbar}\, R(t|\, x, y) - V'(x) y \right) \; R(t) \right\|_{L^2}$$

and

$$\mathcal{D}_4^\hbar(t) \;=\; \left\| \left(\frac{V\left(x + \frac{\hbar}{2}\, y\right) \;-\; V\left(x - \frac{\hbar}{2}\, y\right)}{\hbar} \;-\; \left(V'(x) y + \frac{\hbar^2}{24}\, V^{(3)}(x)\, y^3 \right) \right) \; R(t) \right\|_{L^2},$$

which are respectively of order $\hbar^2$ and $\hbar^4$. Initially this value is small but as the beam approaches the region where the potential is strong, it increases rapidly and the local approximation is not valid anymore.

Finally, we present the time evolution of the Wigner function in phase space, *i. e.* (x,ξ)-space, in Figure 4.11 for $\hbar = 1$. We see that it exhibits a behavior slightly different from the one obtained with $\hbar = 0.1$ since small waves appear and propagate in the phase space domain.

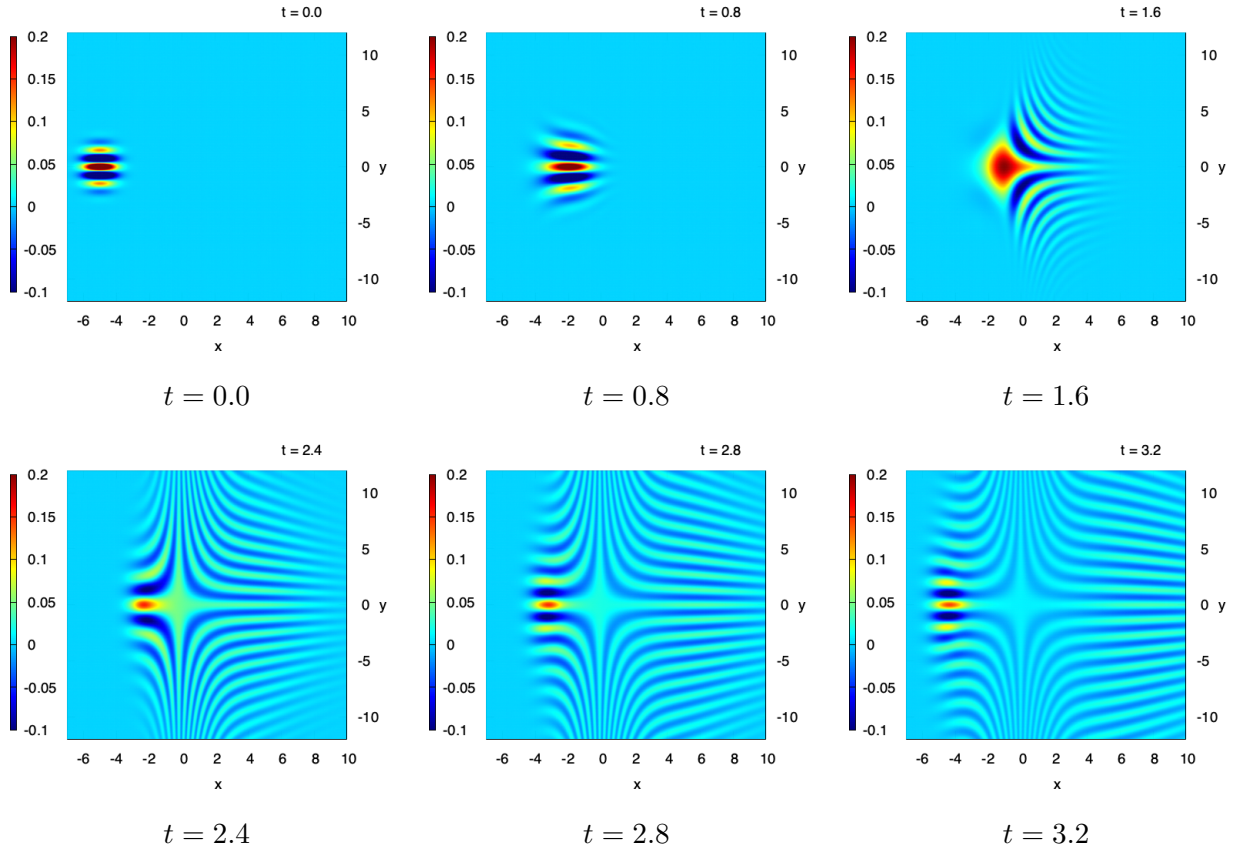

$t = 0.0$ $t = 0.8$ $t = 1.6$

$t = 2.4$ $t = 2.8$ $t = 3.2$

FIGURE 4.7. **Quantum tunneling** : Time evolution of the approximation of $\mathrm{Re}(R)$ with $\hbar = 0.1$.

4.4. **The Morse potential.** The Morse potential is used to approximate the vibrational structure of a diatomic molecule, since it explicitly includes the effects of bond breaking, such as the existence of unbound states. It also accounts for the anharmonicity of real bonds and the non-zero transition probability. The Morse potential energy function is of the form

$$V(x) = 20\ (1 - \exp(-0.16\,x))^2\ ,$$

and the initial datum in the von Neumann equation is

$$R^{in}(x,y)\ =\ \frac{1}{\sqrt{2\pi}\sigma_x}\exp\left(-\frac{1}{2}\left(\frac{(x-x_0)^2}{\sigma_x^2}+y^2\right)\right)\ ,$$

with $x_0 = 4$ and $\sigma_x = 0.6$. Here, the x domain is $[-4, 16]$ with $N_x = 1000$, while $N = 400$, $\Delta t = 0.01$ and $\hbar = 0.5$. We performed again numerical computations using (3.1)-(3.3), with nonlocal term $\mathcal{E}^\hbar$ given by (2.4) and its truncated approximation (3.4) of order $\hbar^4$. Surprisingly both results are in good agreement for the Wigner distribution and the macroscopic quantities (see Figures 4.12 and 4.13).

The time evolution of the Wigner function in phase space is proposed in Figure 4.12 for $\hbar = 0.5$. The initial Gaussian beam is rapidly deviated due to the strong potential. We first see that the trajectory of the beam coincides with the isolines of the Hamiltonian

$$H(x,\xi)\ =\ \frac{\xi^2}{2}\ +\ V(x)$$

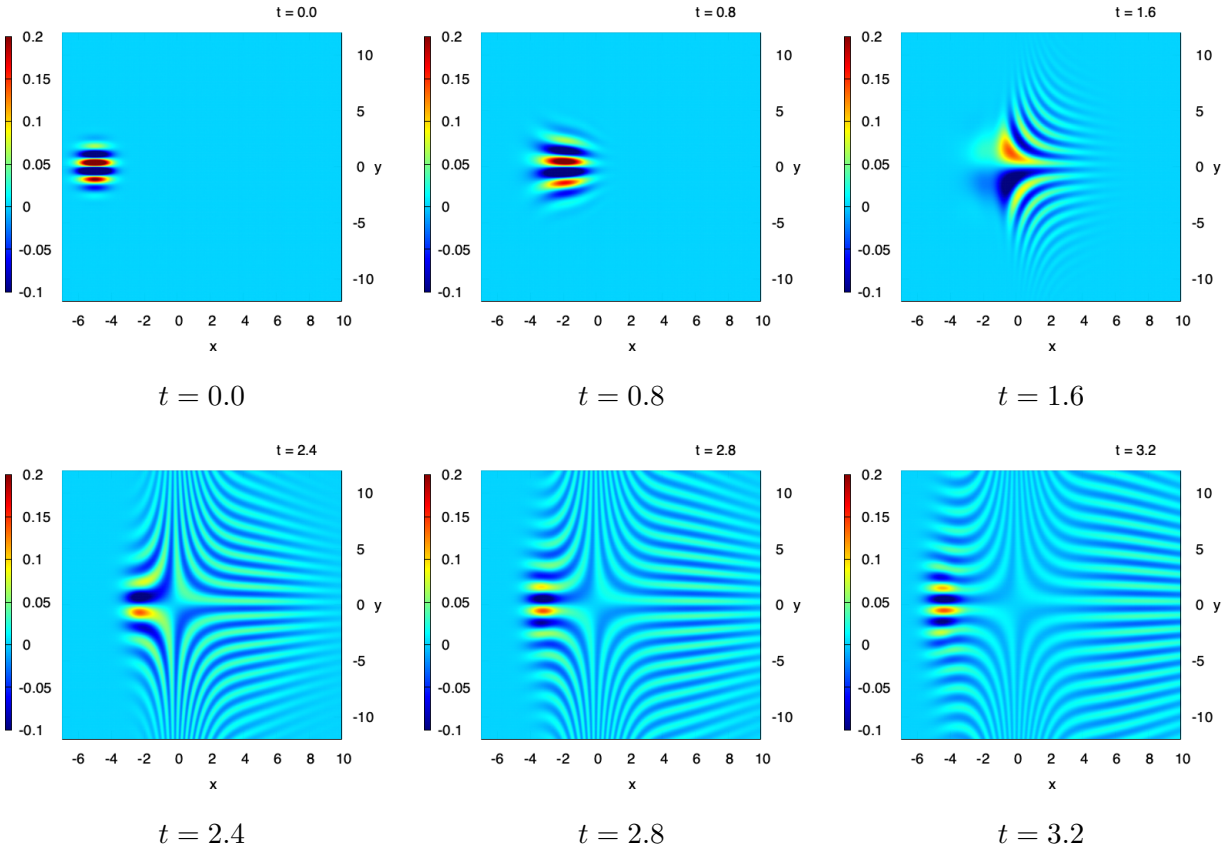

$t = 0.0$ $t = 0.8$ $t = 1.6$

$t = 2.4$ $t = 2.8$ $t = 3.2$

FIGURE 4.8. **Quantum tunneling** : Time evolution of the approximation of $\mathrm{Im}(R)$ with $\hbar = 0.1$.

then the Gaussian beam is distorted and small waves appear in the center and are captured by the strong potential ($t = 20$). These oscillatory waves can be also observed on the density ρ (see left column of Figure 4.13).

5. Conclusion

In conclusion, we have introduced a new approach to discretize the von Neumann equation in the semi-classical limit. By utilizing Weyl's variables and employing a truncated Hermite expansion of the density operator, we are able to address the stiffness associated with the equation. Our method allows for error estimates by leveraging the propagation of regularity on the exact solution. Therefore, our asymptotic preserving numerical approximation, coupled with Hermite polynomials, represents an interesting approach for accurately solving the von Neumann equation in the semi-classical regime. Finally through the development of a finite volume approximation and numerical simulations showcasing phenomena in both quantum mechanics and its semi-classical limit, we have shown the efficiency of the present approach to describe mixed states with smooth Wigner function..

References

[1] G. Allaire, A. Arnold, P. Degond, and T. Y. Hou. *Mathematical properties of quantum evolution equations*. Springer, 2008.

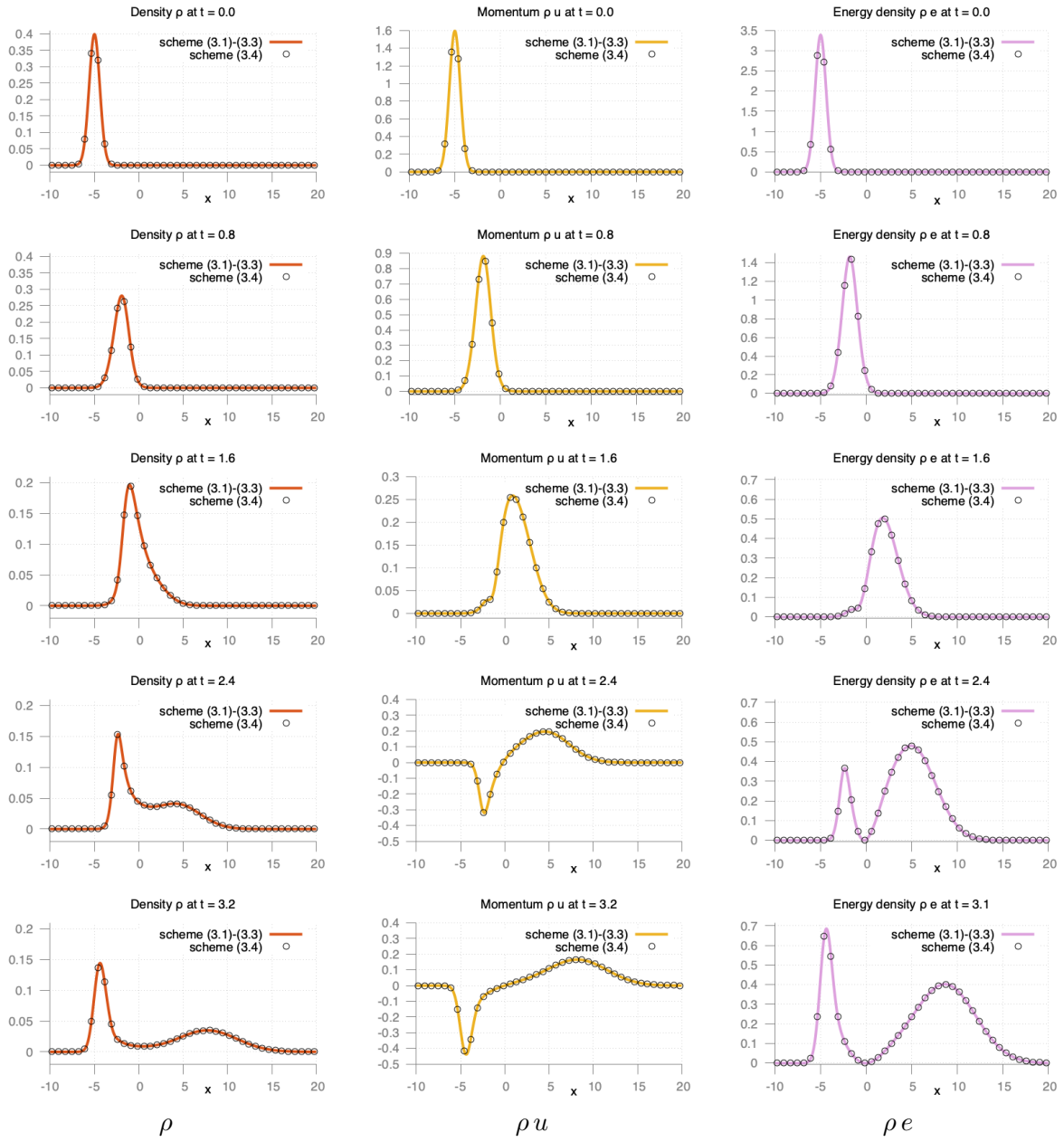

FIGURE 4.9. **Quantum tunneling** : Snapshots of the density ρ, momentum $\rho\, u$ and energy density $\rho\, e$ at time different time. for $\hbar = 0.1$

[2] W. Bao, S. Jin, and P. A. Markowich. On time-splitting spectral approximations for the Schrödinger equation in the semiclassical regime. *Journal of Computational Physics*, 175(2):487–524, 2002.

[3] M. Berman, R. Kosloff, and H. Tal-Ezer. Solution of the time-dependent Liouville-von Neumann equation: dissipative evolution. *Journal of Physics A: Mathematical and General*, 25(5):1283, 1992.

[4] M. Bessemoulin-Chatard and F. Filbet. On the stability of conservative discontinuous Galerkin/Hermite spectral methods for the Vlasov-Poisson system. *J. Comput. Phys.*, 451:Paper No. 110881, 28, 2022.

[5] M. Bessemoulin-Chatard and F. Filbet. On the convergence of discontinuous Galerkin/Hermite spectral methods for the Vlasov–Poisson system. *SIAM Journal on Numerical Analysis*, 61(4):1664–1688, 2023.

[6] A. Blaustein. Structure preserving solver for Multi-dimensional Vlasov-Poisson type equations. 2024.

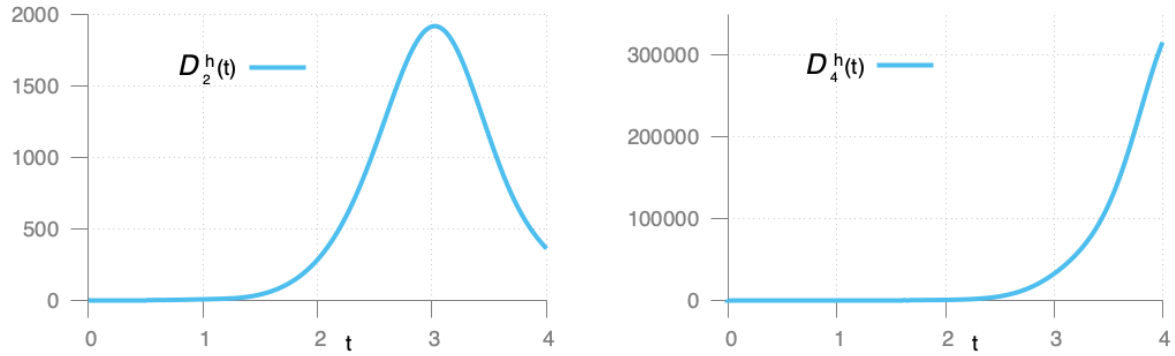

(a) $\mathcal{D}_2^\hbar$ (b) $\mathcal{D}_4^\hbar$

FIGURE 4.10. **Quantum tunneling** : Time evolution of the quantities $\mathcal{D}_2^\hbar$ and $\mathcal{D}_4^\hbar$ for $\hbar = 1$.

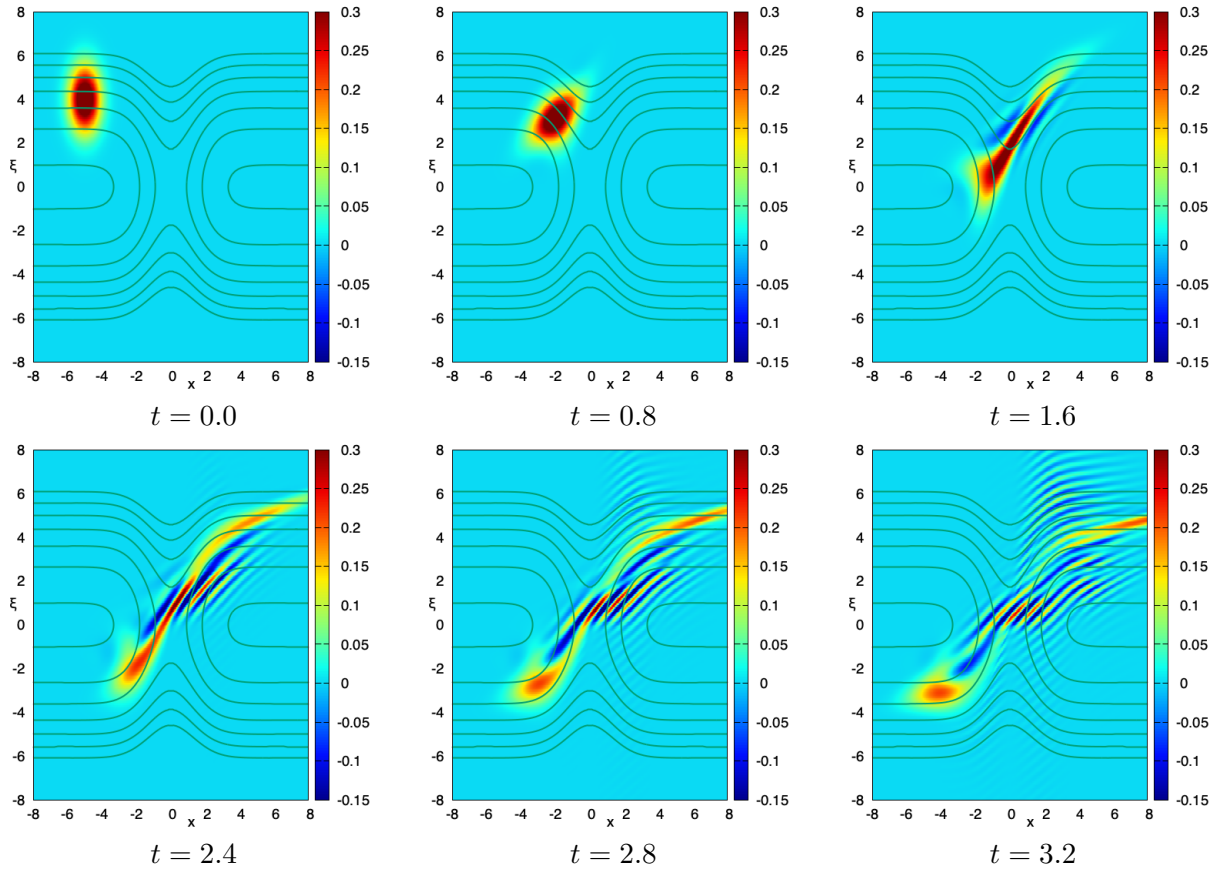

$t = 0.0$ $t = 0.8$ $t = 1.6$

$t = 2.4$ $t = 2.8$ $t = 3.2$

FIGURE 4.11. **Quantum tunneling** : Time evolution of the Wigner function computed from the approximation of R with $\hbar = 1$. The lines represent the level set of the Hamiltonian $H(x, \xi) = V(x) + \xi^2/2$.

[7] A. Blaustein and F. Filbet. A structure and asymptotic preserving scheme for the Vlasov-Poisson-Fokker-Planck model. *Journal of Computational Physics*, 498:112693, 2024.

[8] A. Blaustein and F. Filbet. On a discrete framework of hypocoercivity for kinetic equations. *Mathematics of Computation*, 93(345):163–202, 2024.

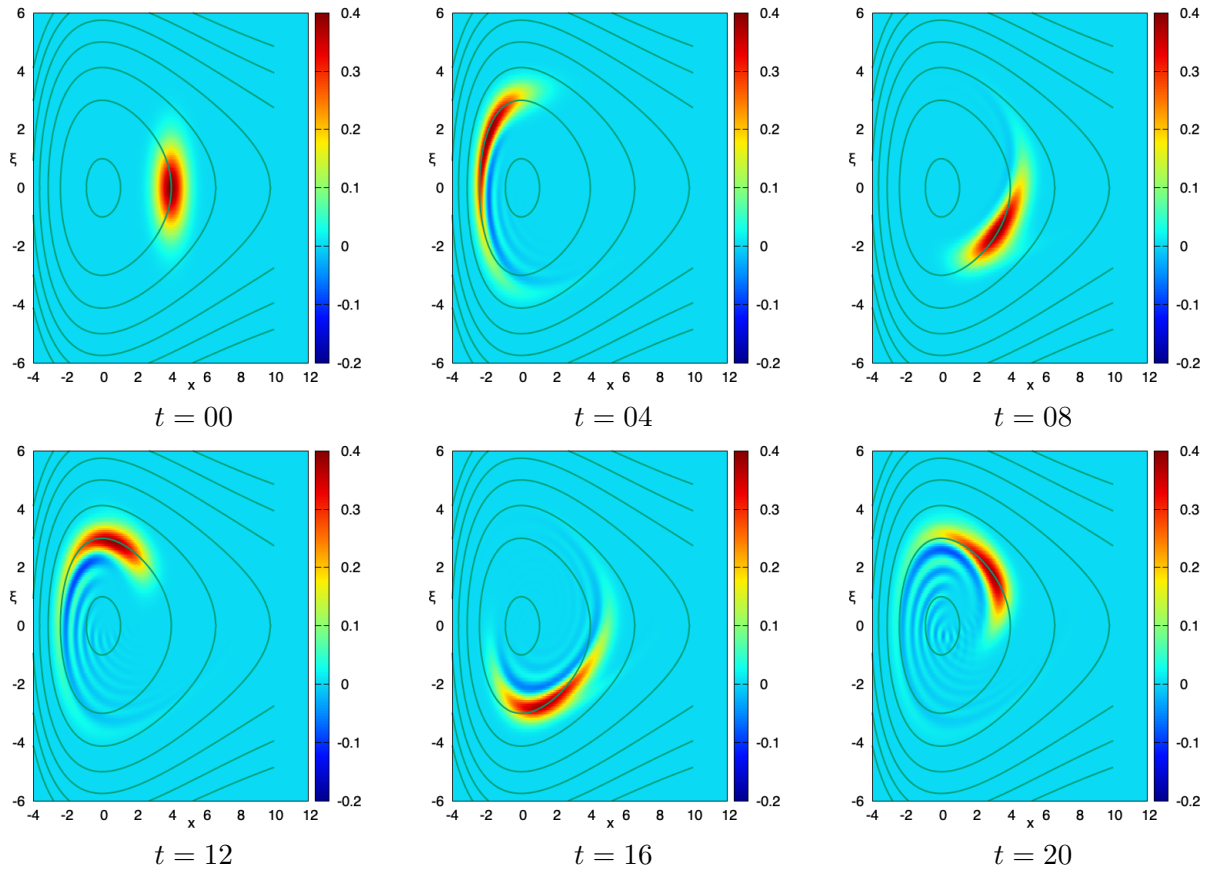

FIGURE 4.12. **Morse potential** : Time evolution of the Wigner function computed from the approximation of R with $\hbar = 0.5$. The lines represent the level set of the Hamiltonian $H(x,\xi) = V(x) + \xi^2/2$.

[9] H. Brézis. *Analyse Fonctionnelle, Théorie et Applications, Masson, Paris, 1983*. (English Translation) Functional Analysis, 2011.

[10] F. Filbet and F. Golse. On the approximation of the von-Neumann equation in the semi-classical limit. Part II : numerical analysis. *preprint*, 2024.

[11] F. Filbet and T. Xiong. Conservative Discontinuous Galerkin/Hermite Spectral Method for the Vlasov–Poisson System. *Commun. Appl. Math. Comput.*, 2020.

[12] F. Golse and M. Jakob. . *preprint*, 2024.

[13] F. Golse, S. Jin, and T. Paul. On the convergence of time splitting methods for quantum dynamics in the semiclassical regime. *Foundations of Computational Mathematics*, 21(3):613–647, 2021.

[14] B. Hellsing and H. Metiu. An efficient method for solving the quantum Liouville equation: Applications to electronic absorption spectroscopy. *Chemical physics letters*, 127(1):45–49, 1986.

[15] J. P. Holloway. Spectral velocity discretizations for the Vlasov-Maxwell equations. *Transport theory and statistical physics*, 25(1):1–32, 1996.

[16] S. Jin. Asymptotic-preserving schemes for multiscale physical problems. *Acta Numerica*, 31:415–489, 2022.

[17] A. Jüngel. *Transport equations for semiconductors*, volume 773. Springer, 2009.

[18] N. Lerner. *Metrics on the phase space and non-self adjoint pseudo-differential operators*, volume 3. Springer Science & Business Media, 2011.

[19] P.-L. Lions and T. Paul. Sur les mesures de Wigner. *Revista matemática iberoamericana*, 9(3):553–618, 1993.

[20] G. Manfredi and M. Feix. Theory and simulation of classical and quantum echoes. *Physical Review E*, 53(6):6460, 1996.

[21] P. A. Markowich and H. Neunzert. On the equivalence of the Schrödinger and the quantum Liouville equations. *Mathematical methods in the applied sciences*, 11(4):459–469, 1989.

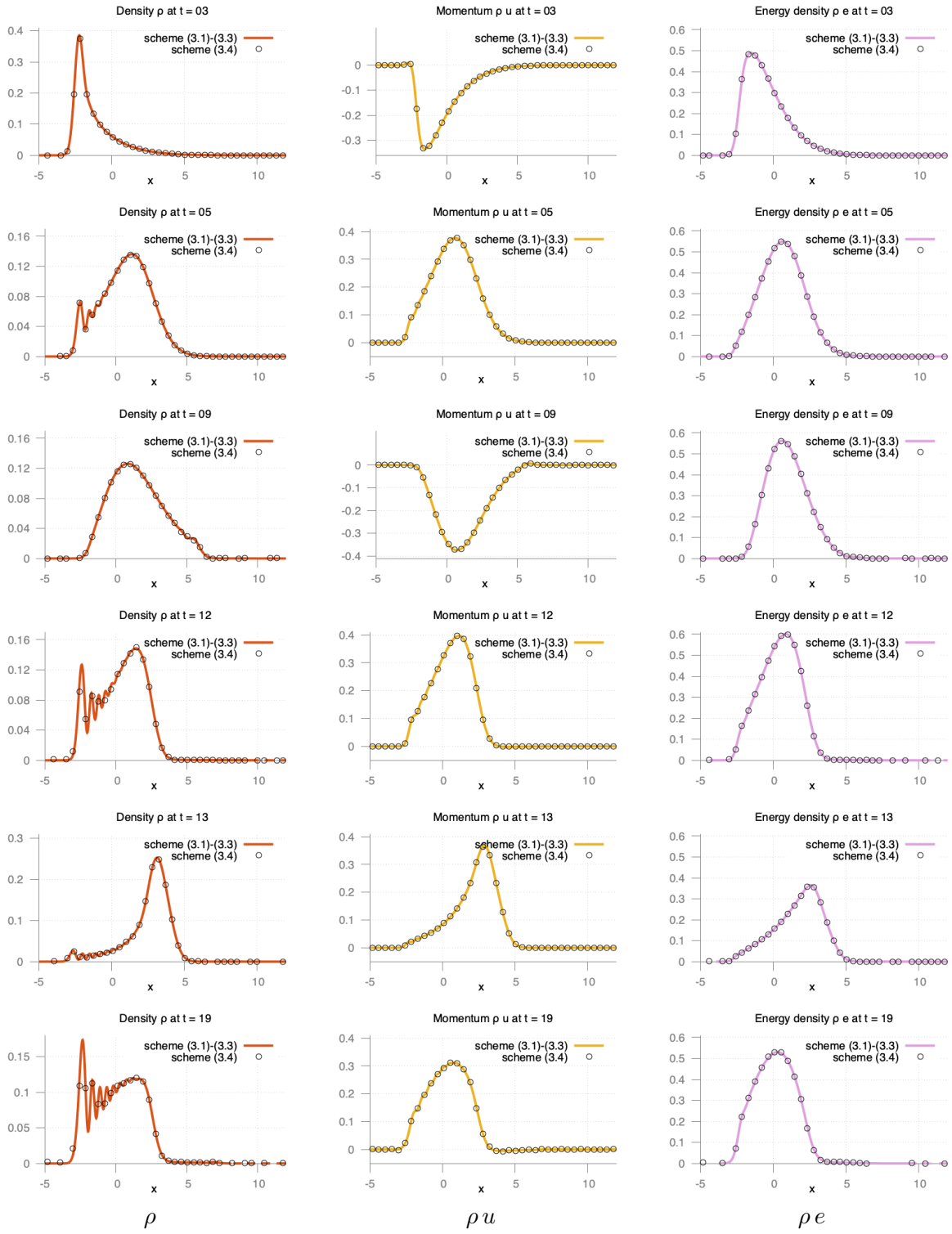

FIGURE 4.13. **Morse potential** : Snapshots of the density ρ, momentum $\rho\ u$ and energy density ρe at time different time. for $\hbar = 0.5$ at time $t = 3$, 5, 9, 12, 13 and 19.

[22] P. A. Markowich, P. Pietra, and C. Pohl. Numerical approximation of quadratic observables of Schrödinger-type equations in the semi-classical limit. *Numerische Mathematik*, 81:595–630, 1999.
[23] P. A. Markowich and C. Ringhofer. An analysis of the quantum Liouville equation. *ZAMM-Journal of Applied Mathematics and Mechanics/Zeitschrift für Angewandte Mathematik und Mechanik*, 69(3):121–127, 1989.
[24] P. A. Markowich, C. A. Ringhofer, and C. Schmeiser. *Semiconductor equations*. Springer Science & Business Media, 2012.
[25] B. Miao, G. Russo, and Z. Zhou. A novel spectral method for the semiclassical Schrödinger equation based on the Gaussian wave-packet transform. *IMA Journal of Numerical Analysis*, 43(2):1221–1261, 2023.
[26] G. Russo and P. Smereka. The Gaussian wave packet transform: Efficient computation of the semi-classical limit of the Schrödinger equation. Part 1–Formulation and the one dimensional case. *Journal of Computational Physics*, 233:192–209, 2013.
[27] G. Russo and P. Smereka. The Gaussian wave packet transform: efficient computation of the semi-classical limit of the Schrödinger equation. Part 2. Multidimensional case. *Journal of Computational Physics*, 257:1022–1038, 2014.
[28] J. W. Schumer and J. P. Holloway. Vlasov simulations using velocity-scaled Hermite representations. *Journal of Computational Physics*, 144(2):626–661, 1998.
[29] J. Sellier, M. Nedjalkov, I. Dimov, and S. Selberherr. A comparison of approaches for the solution of the Wigner equation. *Mathematics and Computers in Simulation*, 107:108–119, 2015.
[30] D. Sels, F. Brosens, and W. Magnus. Wigner distribution functions for complex dynamical systems: A path integral approach. *Physica A: Statistical Mechanics and its Applications*, 392(2):326–335, 2013.
[31] S. Shao, T. Lu, and W. Cai. Adaptive conservative cell average spectral element methods for transient Wigner equation in quantum transport. *Communications in Computational Physics*, 9(3):711–739, 2011.
[32] M. L. Van de Put, B. Sorée, and W. Magnus. Efficient solution of the Wigner-Liouville equation using a spectral decomposition of the force field. *J. Comput. Phys.*, 350:314–325, 2017.
[33] Y. Xiong, Z. Chen, and S. Shao. An advective-spectral-mixed method for time-dependent many-body Wigner simulations. *SIAM Journal on Scientific Computing*, 38(4):B491–B520, 2016.

(F.F.) IMT, Université Paul Sabatier, 31062 Toulouse Cedex, France
Email address: `francis.filbet@math.univ-toulouse.fr`

(F.G.) CMLS, École polytechnique, 91128 Palaiseau Cedex, France
Email address: `francois.golse@polytechnique.edu`